ORIGINAL ARTICLE

**P. R. Spalart · S. Deck · M. L. Shur · K. D. Squires
M. Kh. Strelets · A. Travin**

A new version of detached-eddy simulation, resistant to ambiguous grid densities

Abstract Detached-eddy simulation (DES) is well understood in thin boundary layers, with the turbulence model in its Reynolds-averaged Navier–Stokes (RANS) mode and flattened grid cells, and in regions of massive separation, with the turbulence model in its large-eddy simulation (LES) mode and grid cells close to isotropic. However its initial formulation, denoted DES97 from here on, can exhibit an incorrect behavior in thick boundary layers and shallow separation regions. This behavior begins when the grid spacing parallel to the wall $\Delta_\parallel$ becomes less than the boundary-layer thickness δ, either through grid refinement or boundary-layer thickening. The grid spacing is then fine enough for the DES length scale to follow the LES branch (and therefore lower the eddy viscosity below the RANS level), but resolved Reynolds stresses deriving from velocity fluctuations ("LES content") have not replaced the modeled Reynolds stresses. LES content may be lacking because the resolution is not fine enough to fully support it, and/or because of delays in its generation by instabilities. The depleted stresses reduce the skin friction, which can lead to premature separation.

For some research studies in small domains, $\Delta_\parallel$ is made much smaller than δ, and LES content is generated intentionally. However for natural DES applications in useful domains, it is preferable to over-ride the DES limiter and maintain RANS behavior in boundary layers, independent of $\Delta_\parallel$ relative to δ. For this purpose, a new version of the technique – referred to as DDES, for Delayed DES – is presented which is based on a simple modification to DES97, similar to one proposed by Menter and Kuntz for the shear–stress transport (SST) model, but applicable to other models. Tests in boundary layers, on a single and a multi-element airfoil, a cylinder, and a backward-facing step demonstrate that RANS function is indeed maintained in thick boundary layers, without preventing LES function after massive separation. The new formulation better fulfills the intent of DES. Two other issues are discussed: the use of DES as a wall model in LES of attached flows, in which the known log-layer mismatch is not resolved by DDES; and a correction that is helpful at low cell Reynolds numbers.

Keywords Hybrid RANS/LES · Detached-eddy simulation · Turbulence · Separation

P. R. Spalart (✉)
Boeing Commercial Airplanes, P.O. Box 3707,
Seattle, WA 98124, USA
E-mail: philippe.r.spalart@boeing.com

S. Deck
ONERA, BP 72-29, avenue de la Division Leclerc,
F-92322 Châtillon Cedex, France

M. L. Shur · M. Kh.Strelets · A. Travin
New Technologies and Services (NTS), 197198,
St Petersburg, Russia

K. D. Squires
Department of Mechanical and Aerospace Engineering,
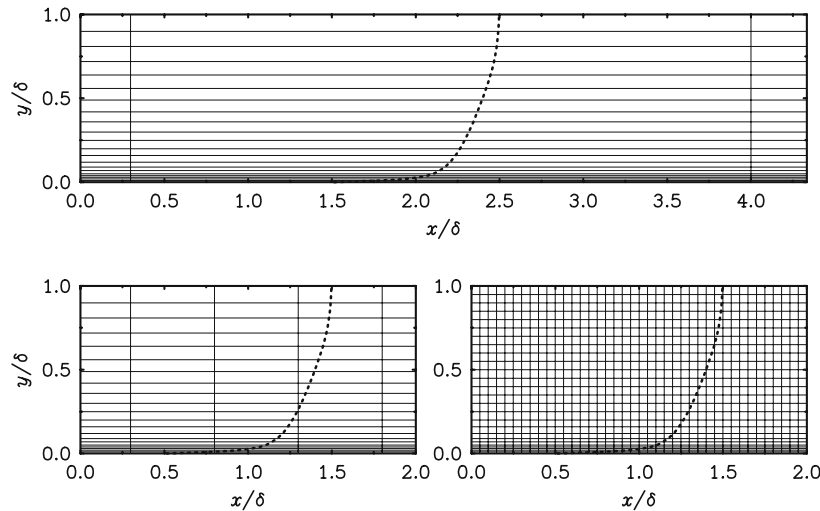Arizona State University, Tempe, AZ 85287, USA

Fig. 1 Grids in a boundary layer. *Top* Type I, natural DES; *left* Type II, ambiguous spacing; *right* Type III, LES. *Dotted lines* mean velocity. δ is the boundary-layer thickness. Assume $\Delta z \approx \Delta x \approx \Delta_{\parallel}$

1 Introduction

Detached-eddy simulation (DES) [1–4] and similar hybrid Reynolds-averaged Navier-Stokes–large-eddy simulation (RANS–LES) approaches are considered promising in high-Reynolds number separated flows by a sizeable community. The use of these techniques is widening, and there have been a wide range of generally successful applications. Predictably, there are also now visible and repeatable imperfections in these studies and it is opportune to examine whether these are structural, or can be traced to inappropriate user actions. Structural issues may be caused by the realities of turbulence physics and therefore permanent (unless DNS is possible), or may be remediable by improvements in the strategy, as is attempted here. Inappropriate user decisions can be slowly limited by user education, primarily via adequate publications and users' manuals [5]. They can be of the type of using much too little computing effort, poor resolution balance between various directions and time, or of attempting a case that is out of reach for fundamental reasons. As an example of the first type, a recurrent mis-conception has been that DES should be applied with a somewhat coarser grid than LES in massive-separation regions and other free shear flows. There is no reason for this, and it is not implied in the core DES papers. DES is not simply "a coarser-grid version of LES." DES differs from LES only in boundary layers, with the model in RANS mode, and then the difference in the required resolutions is very wide, as will be shown shortly. Unfortunately, this unexpected idea has led to several inappropriate comparisons between LES and DES [6, 7].

Detached-eddy simulation(DES) as originally proposed is designed to treat the entire boundary layer using a RANS model and to apply an LES treatment to separated regions. This constitutes the "natural" use of the method and another objective here is to classify the imperfections mentioned above between those which affect DES in its intended, natural, mode of operation, and those which appear only in derivative uses of the DES equations or in extensions of the initial "vision." The latter are deferred to Sect.4. For natural DES, the issues can be loosely attributed to the existence of a "grey area" between the RANS and LES regions, announced from the outset in 1997 [1], but left for future thinking. We now have 8 years of experience and critiques from numerous groups. The new version of DES – DDES – addresses precisely these natural applications.

To motivate DDES, Fig. 1 displays three grid densities in a boundary layer. For ease in explanation, recall the basic formulas of DES when based on the Spalart–Allmaras (S–A, [8]) model for the length scale $\tilde{d}$ that enters the turbulence model and controls the eddy viscosity: $\tilde{d} \equiv \min(d, C_{\mathrm{DES}}\Delta)$, where d is the wall distance, C_{DES} is of order 1, and $\Delta \equiv \max(\Delta x, \Delta y, \Delta z)$ is the chosen measure of grid spacing (the preference between this measure and others such as $(\Delta x \Delta y \Delta z)^{1/3}$ is a separate issue, present in any LES [9]).

In a Type I grid, typical of RANS and of DES with a thin boundary layer, the wall-parallel spacings Δx and Δz set Δ via the max formula and exceed δ, so that the DES length scale is on the "RANS branch" (i.e., $\tilde{d} = d$) throughout the boundary layer. The model functions as intended, since DES was created precisely to by-pass LES in large areas of thin boundary layer.

The other extreme is the Type III, LES grid, with all spacings much smaller than δ ($\Delta \approx \delta/20$ makes a plausible starting value [1], but $\Delta \approx \delta/10$ gives acceptable results). The model functions as a sub-grid scale (SGS) model (i.e., $\tilde{d} = C_{\mathrm{DES}}\Delta$) over the bulk of the boundary layer, and as a RANS-like wall model very near the wall ($\tilde{d} = d$), with a grey layer in-between. This regime is a type of wall-modeled LES (WMLES). LES started with wall modeling in the 1970s, then moved away from true wall modeling when computing power allowed the resolution of the near-wall streaks, and is now tentatively returning to wall modeling as the demand for high Reynolds numbers mounts [10]. This has proven very challenging, and a number of rather complex solutions have been proposed in the literature. Using a Type-III grid with adequate initial or inflow LES content represents a derivative use of the DES formulas, as discussed by [11] and here in Sect. 4.1. Although quantitatively not perfect, this approach has merits including simplicity and stability, and responds well to Reynolds-number and grid-density variations.

The "ambiguous" grid of Type II unfortunately activates the DES limiter ($\tilde{d} = C_{\mathrm{DES}}\Delta$) roughly in the upper two-thirds of the boundary layer, but is patently not fine enough to support resolved velocity fluctuations internal to the boundary layer, i.e., LES content. The DES limiter then reduces the eddy viscosity, and therefore the modeled Reynolds stress, without any sizeable resolved stress to restore the balance [1]. This will be referred to as modeled-stress depletion (MSD). It occurs if the grid is gradually refined starting from Type I, typically when a user is justifiably seeking grid convergence, or when geometry features demand a fine wall-parallel grid. It also occurs when a boundary layer thickens and nears separation. Thus, over an airfoil, the same grid may be of Type I at one angle of attack, and of Type II at another angle.

Modeled stress depletion(MSD) was predicted from the origin of the method [1], though anticipated only with "excessive" grid refinement and therefore not perceived as a major issue. The initial demonstrations of the technique were over applications such as thin airfoils, which are not sensitive to the grey area [2]. A subsequent detailed study on the circular cylinder was also free of grid problems even with grid refinement, because that flow has neither geometrical incentives for fine wall-parallel grid spacing (low $\Delta_\parallel$), nor thick boundary layers (high δ) [3]. These factors retarded the recognition of the ambiguous-grid issue. It was then encountered in studies of Caruelle [12] and Deck [13], and strongly emphasized by Menter and Kuntz [14] who showed how severe cases of MSD lead to "grid-induced separation," although with 2D examples which were somewhat artificial. Therefore it was important to determine whether affordable 3D grids can lower $\Delta_\parallel$ in both directions sufficiently to result in MSD. This has proven to be the case, particularly in boundary layers gradually approaching separation, when δ can reach 10% of the airfoil chord [7] (see Sect.3.4). This deficiency needs to be addressed if DES is to be reliable in its natural mode with a variety of grid spacings, adapted to geometry or shock waves, and boundary-layer thicknesses.

The issue of MSD faces any hybrid RANS–LES method, such as limited numerical scales (LNS) [15], that aims at a function akin to natural DES and introduces the grid spacing into the turbulence model in order to achieve an LES treatment. In contrast, two recently proposed methods, scale-adaptive simulation (SAS) and turbulence-resolving RANS (TRRANS), do not use the grid spacing [16,17]. These methods are based on pure RANS models, but exhibit some LES properties: both achieve LES behavior in simulations of homogeneous turbulence. However, neither approach has been able to sustain LES content in a channel, and TRRANS fails to sustain unsteadiness over a backward-facing step, normally an excellent candidate for hybrid methods (Sect.3.5). Thus, the control between RANS and LES function is not fully understood, and the role played by differencing errors may be powerful. On the other hand, both methods are very young, and this understanding may improve soon.

An initial solution to MSD was proposed, and is to make the DES "zonal:" the C_{DES} limiter is disabled in selected regions, where an attached boundary layer is expected [18]. This "manual reversion" is adequate in simple geometries, but defining such regions in realistic 3D multi-body cases would be lengthy and error-prone, so that this solution is not sufficient in general, and a case-independent formulation change is much preferred. This has prompted non-zonal attempts, which have been only partly successful and thus should be superseded by DDES, assuming its validation continues without major setbacks.

One such proposal is to use the aspect ratio of the grid cells (cf. Fig. 1). An aspect ratio much larger than unity signals a boundary layer, and the length scale $\tilde{d}$ can be biased upwards, so as to favor RANS mode. This was exercised by Dr. J. Forsythe in collaboration with the authors, but does not appear to be a robust solution, at least in the unstructured grids that were used. The bias delays the switch to the LES branch, but the aspect ratios are not usually large enough to give a clear enough "signal," leading to manual adjustments as different grids are used. In addition, many unstructured grids have abrupt transitions from high-aspect-ratio hexahedral cells near walls to low-aspect ratio tetrahedral cells away from walls, which would cause abrupt switching

between modes (Δ is less noisy). Conversely, structured grids tend to have regions with unnecessarily fine and high-aspect ratio cells outside boundary layers, causing further damage to this concept.

A similar modification was used by Forsythe et al. [19], who found it more satisfactory, although the same objections can be made (tendency to re-adjustments, and sensitivity to jumps in cell types). The idea is to replace the DES97 length scale $\min(d, C_{\mathrm{DES}}\Delta)$ with a function $\tilde{d}(d, C_{\mathrm{DES}}\Delta)$ that has the same limiting behaviors when $d \ll C_{\mathrm{DES}}\Delta$ and when $d \gg C_{\mathrm{DES}}\Delta$, but keeps following d when it is only somewhat larger than $C_{\mathrm{DES}}\Delta$ (DDES achieves this behavior via different means). Specifically, these investigators implemented $\tilde{d} \equiv \min(C_{\mathrm{DES}}\max(n^2 C_{\mathrm{DES}}\Delta^2/d, \Delta), d)$, with $n = 3$. This extends RANS behavior to a thicker layer. However, the use of the ratio $d/(C_{\mathrm{DES}}\Delta)$ to identify boundary layers is not much more robust than the use of cell aspect ratio. In general, the user cannot be expected to anticipate the thickness of the boundary layer at grid-generation time, especially with incipient separation. Grid adaptation solves this problem, but present automatic grid-adaptation algorithms produce strong local variations of cell size and aspect ratio.

A solution within the DES equations was proposed by Menter and Kuntz [14] who use the F_2 or F_1 functions of the SST two-equation RANS model to identify the boundary layer, and prevent a switch to LES. The DDES solution proposed here is a derivative of their proposal, but is not limited to the SST model; it is general, as long as the model involves an eddy viscosity. It is presented in Sect. 2, and exercised in Sect. 3. Then, Sect. 4 discusses wall-modeled LES and introduces a low-Reynolds number correction which, roughly, extends DES to flows at laboratory Reynolds numbers. Finally, Sect. 5 is devoted to the outlook for DDES.

2 DDES formulation

2.1 Presentation

As mentioned above, Menter and Kuntz [14] use the blending functions F_2 or F_1 of the SST model to "shield" the boundary layer, by which they implied "preserve RANS mode," or "delay LES function." Except for a low-Reynolds number limiter, the argument of these functions is $\sqrt{k}/(\omega y)$, which is the ratio between the internal length scale $\sqrt{k}/\omega$ of the k-ω turbulence model and the distance to the wall (d, or y). The F functions equal 1 in the boundary layer, and fall to 0 rapidly at the edge. One-equation models such as S-A do not have an internal length scale, but involve the parameter r which is also the ratio (squared) of a model length scale to the wall distance (the length scale is not internal in that it involves the mean shear rate). For DDES, the parameter r is slightly modified relative to the S-A definition, in order to apply to any eddy-viscosity model, and be slightly more robust in irrotational regions:

$$r_{\mathrm{d}} \equiv \frac{\nu_t + \nu}{\sqrt{U_{i,j}U_{i,j}}\kappa^2 d^2}, \tag{2.1}$$

where ν_t is the kinematic eddy viscosity, ν the molecular viscosity, $U_{i,j}$ the velocity gradients, κ the Kármán constant, and d the distance to the wall. Similar to r in the S-A model, this parameter equals 1 in a logarithmic layer, and falls to 0 gradually towards the edge of the boundary layer. The addition of ν in the numerator corrects the very near-wall behavior by ensuring that r_{d} remains away from 0. In the S-A model, $\tilde{\nu}$ can be used instead of $\nu_t + \nu$. The subscript "d" represents "delayed."

The quantity r_{d} is used in the function:

$$f_{\mathrm{d}} \equiv 1 - \tanh([8r_{\mathrm{d}}]^3), \tag{2.2}$$

which is designed to be 1 in the LES region, where $r_{\mathrm{d}} \ll 1$, and 0 elsewhere (and to be insensitive to r_{d} exceeding 1 very near the wall). It is similar to $1 - F_2$, and rather steep near $r_{\mathrm{d}} = 0.1$.

The values 8 and 3 for the constants in (2.2) are based on intuitive shape requirements for f_{d}, and on tests of DDES in the flat-plate boundary layer (Sect. 3.2). These values for the coefficients ensure that the solution is essentially identical to the RANS solution, even if Δ is much less than δ. A value larger than 8 would delay LES in even larger regions, which would be safer in the sense of avoiding MSD, but is undesirable overall. It is conceivable that models very different from S-A would make r_{d} approach 0 at $d = \delta$ differently enough to require a modest adjustment of f_{d}.

The application of the above procedures to S-A-based DES, which is used from here on, proceeds by re-defining the DES length scale $\tilde{d}$:

$$\tilde{d} \equiv d - f_{\mathrm{d}} \max(0, d - C_{\mathrm{DES}}\Delta). \tag{2.3}$$

Setting f_{d} to 0 yields RANS ($\tilde{d} = d$), while setting it to 1 gives DES97 ($\tilde{d} = \min(d, C_{\mathrm{DES}}\Delta)$). Several applications shown below will display the f_{d} distribution.

For DES based on most of the possible RANS models, DDES will consist in multiplying by f_{d} the term that constitutes the difference between RANS and DES, just as in (2.3).

2.2 Interpretation

This new formula (2.3) for $\tilde{d}$ does not represent a minor adjustment within DES; there is a qualitative change. Without it, $\tilde{d}$ depends only on the grid; with it, the length scale now also depends on the eddy-viscosity field. It is time-dependent. The issue is not with coding the equations. The crucial effect is that RANS function is self-perpetuating, i.e., the model using (2.3) for $\tilde{d}$ can "refuse" LES mode if the function f_{d} indicates that the point is well inside a boundary layer, as judged from the value of r_{d}. However, if massive separation occurs, f_{d} does rise from 0, and LES mode takes over; verifying this is an essential task in this paper. In fact, the switch from RANS to LES takes place more abruptly following separation than in DES97, which is desirable; the grey area between RANS and LES is narrower. This does not in itself create LES content, but it accelerates its growth following natural instabilities, closer to the region where modeled Reynolds stresses are still at full strength.

Note that the provision of a protection against ambiguous grids does not remove the burden on DES users to generate adequate grids [5], which is far from trivial in complex flows, and to conduct meaningful grid refinements, except in repetitive series of cases (for instance, simulations of slightly different aircraft or vehicles, with the same topology and flow features). Grid quality must be established in any publication, and unfortunately it is easy to abuse the robustness of any approach.

A full solution to the MSD issue would also address free shear layers, which the F_2 and f_{d} functions do not (Sect. 3.6). One reason to leave these for further work and publish the present DDES formulation is that DES grids are normally fairly isotropic outside boundary layers [5], and therefore not of Type II. Consequently, the grid is either fine enough to sustain an LES of the shear layer, or so coarse that it smears it, and an accurate solution is simply not to be expected irrespective of the eddy viscosity. In addition, shear layers sustain instabilities even on wave-lengths much larger than their thickness, unlike boundary layers; this allows some LES content to be generated even with residual RANS-like eddy viscosity, albeit slowly since the growth rate is the inverse of the wave-length. A substantial challenge is that any solution to MSD for free shear layers should provide that the entire layer switches from one mode to the other at once, which is difficult to obtain using local quantities.

3 DDES tests

3.1 Overview

The intent is to exercise DDES widely enough to be able to recommend it with confidence over DES97. It is easy to demonstrate an improvement in a simple case "designed" to suffer MSD, but more difficult to anticipate cases in which the new version would in fact be less capable than the old. If a class of such cases exists, the danger is that the two versions will co-exist in the community, which will lead to waste of effort and impede comparisons. Another objective is to exercise DDES in separate codes, which would help detect any special difficulty, or ambiguity in the formulation. Two codes are used here; DDES was successfully implanted in a third, but its results are not used. Next the two codes, which do not share any modules, are briefly described.

The NTS CFD code used in Sects. 3.2–3.5 provides the capability of steady RANS computations and time-accurate simulations of turbulent flows in the framework of different approaches (URANS, DES, SAS, TRRANS, LES, and DNS). The code accepts structured multi-block overset grids and employs finite-volume approximations based on the implicit flux-difference splitting scheme of Rogers and Kwak for incompressible flows and Roe's scheme for compressible flows. In the steady and unsteady RANS computations, the inviscid fluxes are approximated with upwind-biased third- or fifth-order accurate differences and the viscous fluxes with centered second-order differences. In DES97 and DDES, a hybrid (fifth-order upwind/fourth-order centered) approximation is used with a blending function dependent on the solution [20]. Time integration
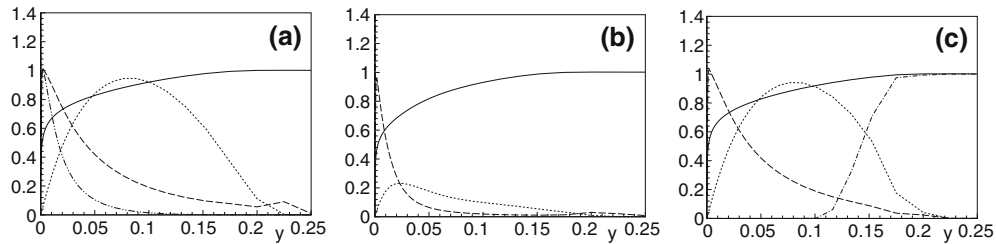
Fig. 2 Distributions in flat-plate boundary layer. **a** Reynolds-averaged Navier–Stokes (RANS). **b** Detached-eddy simulation 97(DES97). **c** DDES. Unit Reynolds number 10^6, $R_x = 1.2 \times 10^7$ (fine grid starting at $R_x = 10^7$), $R_\theta \approx 1.8 \times 10^4$; $\Delta_\parallel \approx 0.1\delta$. —, U/U_∞ (**a, b, c**); $\cdots$, $0.002\,\mu_t/\mu$ (**a, b, c**); - - -, r or r_d (**a, b, c**); - - —- - -, $Dest/(4c_{b1}\tau_w)$ (**a**); - —- -, f_d (**c**)

is performed with the second-order accurate three-layer backward scheme. At every time step the resulting finite-difference equations are solved with the use of Gauss–Seidel relaxations by planes and sub-iterations in "pseudo-time."

The code FLU3M used in Sect. 3.6 also accepts multi-block structured grids, but is second-order accurate for all terms, using a finite-volume approach and a modified AUSM+(P) upwind scheme [18]. Time integration uses a second-order Gear formulation, with an LU factorization of the implicit system.

3.2 Boundary layers

Figure 2 compares RANS, DES97 and DDES in a boundary layer with grid spacing about 1/10th of the boundary-layer thickness; this is a strong case, more severe than in Fig. 1, and the ambiguous-grid region penetrates deep into the boundary layer. Indeed, with DES97 (Fig. 2b) the peak eddy viscosity is reduced by about 75%, and the skin friction by 19% from the RANS prediction, an echo of a similar test in the initial DES paper [1]. In contrast, DDES preserves the eddy viscosity almost fully. Note that f_d can safely rise from 0 in the upper half of the boundary layer, because the S-A destruction term is already negligible in that region (Fig. 2a). The small deficit of eddy viscosity at the edge is very acceptable. It could be eliminated by slanting the f_d function towards more "shielding," but at some point it would suppress LES behavior where such behavior is best. These considerations guided preliminary tests, not shown here, that were used to choose the coefficients for f_d. Another boundary-layer test with an even finer grid was similarly satisfactory.

3.3 Circular cylinder

The case listed as LS2 by Travin et al. [3] was run again with the expectation that DDES would agree with DES97, which was quite successful. It has laminar separation (treated with the Trip-Less mode of the S-A model), Reynolds number 10^5, and a fairly coarse grid with the spanwise grid spacing of 0.07 diameters setting Δ in the near-wake. Flow visualizations, not shown, reveal that DDES has little impact on the eddy viscosity in the separated shear layer, and on the evolution of the layer. Presumably, the destruction term is already weak in this flow, due to the eddy viscosity growing only well downstream of laminar separation. Figure 3 confirms that the quantitative effect on the pressure is insignificant. The structure of DDES strongly suggests that the fine grid would return the same behavior.

3.4 Single airfoil

This airfoil was studied experimentally by Gleyzes and Capbern [22], at Reynolds number 2.1×10^6 and angle of attack $13.3°$. With its sustained adverse pressure gradient, it is a prime example of a boundary layer thickening sufficiently to damage the RANS mode of DES97 even on a grid of medium density, as δ reaches around 7% of the chord, or 14 times $\Delta_\parallel$ (Fig. 4a). The separation is very mild, and the simulation is run without LES-content generation. Therefore, the desirable behavior is for RANS mode to extend to the trailing edge. This is indeed obtained with DDES, as shown by Fig. 4. The f_d function is close to 0 over almost the entire region marked by eddy viscosity (Fig. 4b,c). Its behavior is unremarkable, with a steep rise from 0 to 1, but the small region in which it imposes RANS mode is the key region in this flow. Figure 5 confirms that Grid-Induced
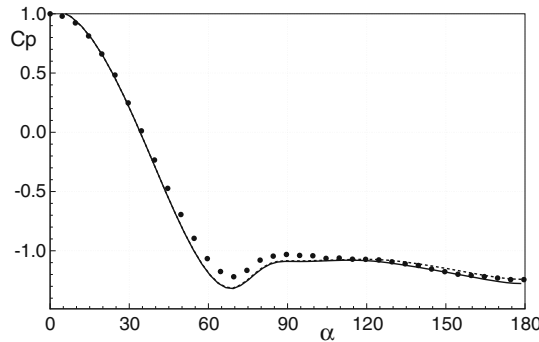
Fig. 3 Pressure distributions on circular cylinder.*Continous line* DES97; *dashed line* DDES; filled Circles experiment [21]
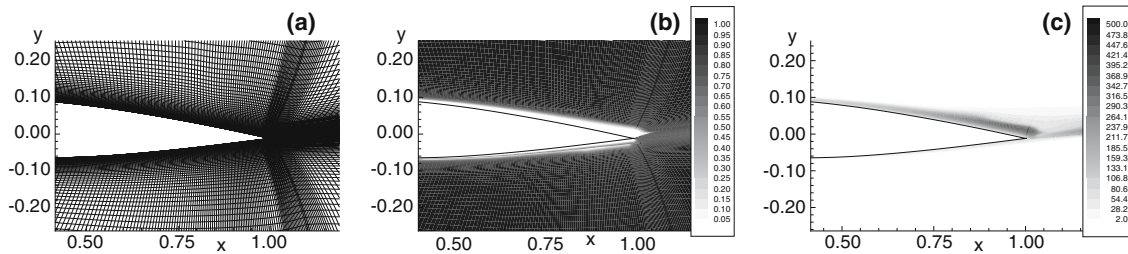

Fig. 4 DDES over A airfoil. **a** Grid ($\Delta z < \Delta x \approx 0.005$, 412 points around airfoil). **b** f_d function. **c** eddy viscosity
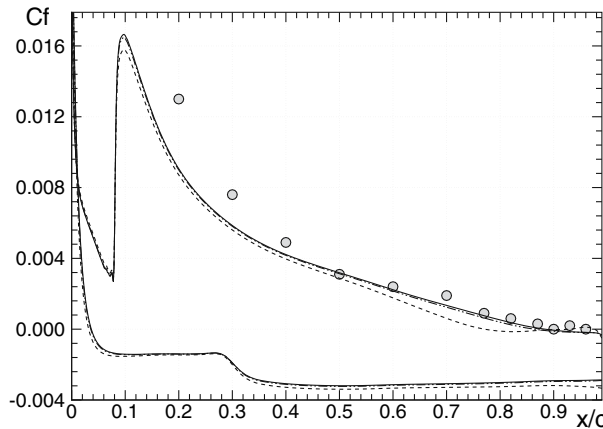

Fig. 5 Skin-friction coefficient over a airfoil.—, RANS; - - -, DES97; - — -, DDES; ○, experiment

Separation at $x/c = 0.77$ has been corrected by the f_d term. The experiment is shown for reference, but the emphasis is on preventing hidden grid-induced alterations of the solution, starting from RANS mode. Perfect agreement is not to be expected, for reasons which include the imperfections of the RANS model, and 2D and 3D wall effects. In addition, the upper-surface boundary layer in these simulations was tripped slightly ahead of the laminar separation near $x/c = 0.08$, which helps convergence but somewhat damages the C_f farther downstream.

3.5 Backward-facing step (BFS)

This is a key case, in that the desired behavior from DES is to maintain RANS mode in both attached boundary layers (i.e., the entire opposite wall, and the step side for $x < 0$), while switching to LES mode as rapidly as possible after separation from the corner, without input perturbations. DES97, with a sensible grid refinement near the step, suffers from ambiguous behavior. This is benign for the boundary layer approaching the step:
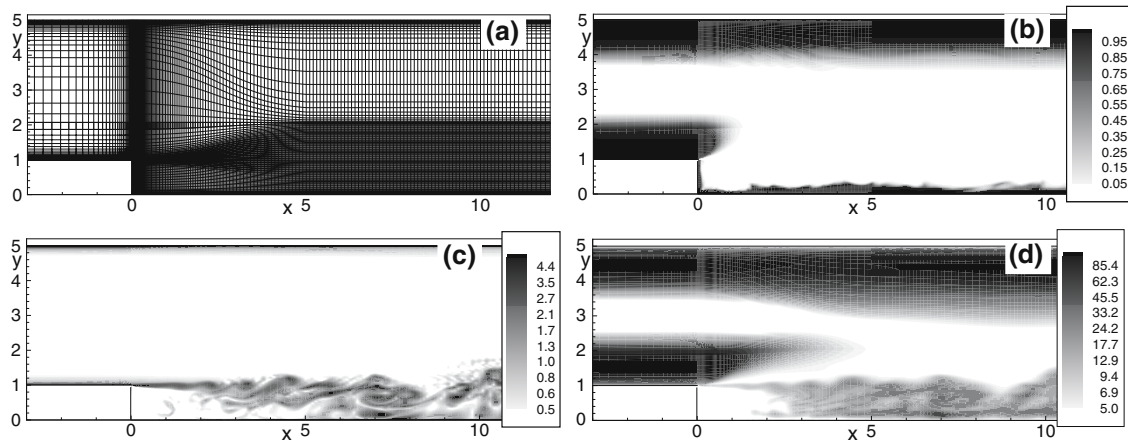
Fig. 6 DDES over backward-facing step. **a** Grid ($\Delta z = 0.03h$, period $\lambda_z = 2h$). **b** $1 - f_\mathrm{d}$ function. **c** Vorticity. **d** eddy viscosity **c** and **d** have non-linear scales for contours levels
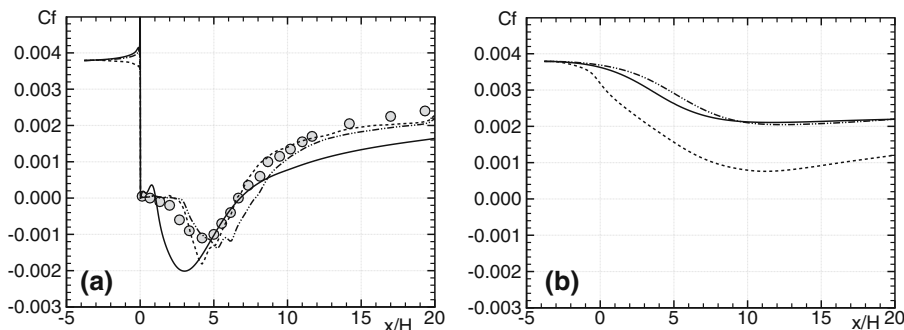

Fig. 7 Skin-friction coefficient in DES over backward-facing step. **a** Step side. **b** Opposite side. ○, experiment [23]; —, RANS; - - -, DES97; - — -, DDES

the skin friction becomes grid-sensitive, but separation of course takes place at the step. The opposite-wall boundary layer is more troublesome, because it needs to resist separation in the adverse pressure gradient, and to produce an accurate thickness evolution. Figure 6 shows details of the DDES solution, and confirms that both qualitative objectives are reached. As expected, the variations of f_d are rather steep, but not enough to cause numerical difficulties. The lower levels of eddy viscosity in the LES region than in the RANS regions are vividly seen. Figure 7 shows skin friction, for RANS, DES97, and DDES. Its behavior is convincing in that the step-side skin friction remains accurate in DDES, while the grid-induced drop by up to 60% on the opposite side is eliminated. The known accuracy advantage of DES over RANS (at least, over RANS using the S-A model) after separation is preserved.

Figure 8 expands the comparison between DES97 and DDES, showing that LES content is essentially as fine with either approach, both in the free shear layer and in the reattaching wall layer. In other words, they use the grid equally well, which is not obvious based on the formulation since the DDES equations tend to inflate the eddy viscosity, relative to DES97. This flow demonstrates the ability of DDES to continue LES behavior in a boundary layer, and this is also the case in a channel. The BFS re-developing region is an example of co-existence of the RANS and LES modes, as long as the two boundary layers remain distinct. Much farther downstream, the two boundary layers will eventually make contact, and the entire channel will adopt a single mode. This was emulated in a temporally-evolving channel (which is much less costly than a very long spatially-developing one), by creating a RANS initial field near one wall and an LES initial field near the other wall. The boundary layers then gradually thickened, each in its own mode. The outcome was that LES mode "invaded" RANS mode, propagating LES content and reducing eddy viscosity. This is satisfactory, considering that the grid was of Type III, so that the computing cost was that of an LES. However, the other possible outcome, namely an "invasion" by RANS, would not have been catastrophic since the S-A RANS model is quite accurate in the channel; it would simply have led to a waste of computing effort.
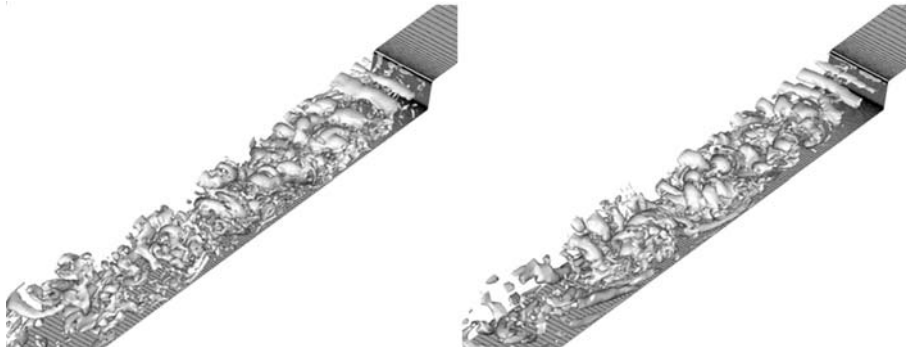
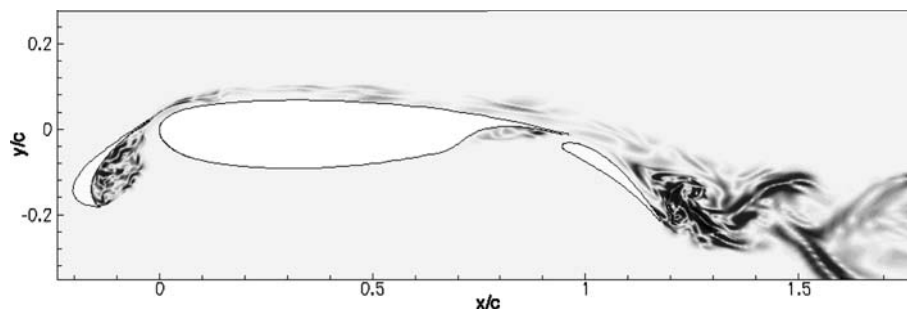**Fig. 8** Swirl contours in backward-facing step flow. *Left* DES97; *right*, DDES

Fig. 9 Flow over a multi-element airfoil. Contours of spanwise velocity

3.6 Multi-element airfoil

This is the most complex geometry, and a good outcome would be a positive indicator for industrial applications of DDES. This flow exhibits large low speed areas, strong pressure gradients, confluence of boundary layers and wakes, and unsteadiness and three-dimensionality on fairly large scales. Each of these can create a challenge for a hybrid RANS/LES calculation. The needs of the different regions place conflicting demands on the grid, especially since it is structured. The chord Reynolds number is 1.8×10^6; the $x-y$ grid has 250,000 points, and the spanwise grid has 31 points with $\Delta z/c = 0.002$. This makes the spanwise period appear small at 6% of c, but at this angle of attack, it should be compared with the chords of the slat and flap, rather than that of the airfoil. The time step is $2.2 \times 10^{-5} c/U_\infty$. This resolution far exceeds what would be feasible for an entire wing today (however, somewhat coarser resolutions, soon to be feasible for such cases, would also experience MSD).

In Fig. 9, three regions with reversed flow, namely the slat cove, the flap cove, and the wake over the flap, sustain LES content even with the f_d correction, again indicating that it is not too strong. The slat wake inherits some LES content from the cove, but it is highly elongated by the acceleration, and the wake is much too thin for LES mode to flourish in the present grid. Such a reversion from LES to RANS is tolerable when the shear layer which suffers it is not dominant, but this illustrates the robustness that will be needed from hybrid methods in real-life applications, and the potential for mode changes in either direction between RANS and LES in each region of such complex flows, as the grid is refined. In fact, this slat wake combined with the main-element wake *can* become dominant at other angles of attack, when off-surface reversal begins over the flap, and drastically alters its lift.

Figure 10 presents velocity and eddy-viscosity profiles of the boundary layer in the vicinity of the main-element trailing edge. At this station, the boundary layer has thickened, and the grey area penetrates deeply into it. Note how the eddy viscosity of DES97 is dramatically reduced compared to RANS, as in Fig. 2. In contrast, DDES preserves the eddy viscosity in the wall layer. The outer part of the boundary-layer profile is influenced by the merging with the slat wake, which is treated neither in full RANS mode nor in LES mode (recall Sect. 2.2). Note how the slat wake near $d/c = 0.045$ is narrower with DDES than with RANS, presumably a case of MSD, although unsteady wavering would result in a wider wake in the time average. This is confirmed by Fig. 11a, which presents the evolution of $1 - f_d$ near the wall, and other quantities relevant to DDES. One can
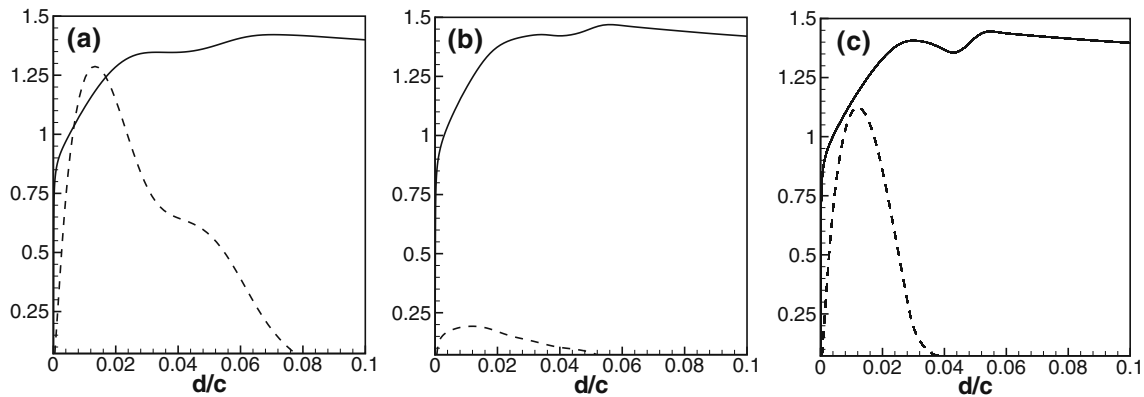
Fig. 10 Distributions in boundary layer over the main element at $x/c = 0.95$: **a** RANS. **b** DES97. **c** DDES *Continuous line*, U/U_∞; *dashed line* $0.005\mu_t/\mu$
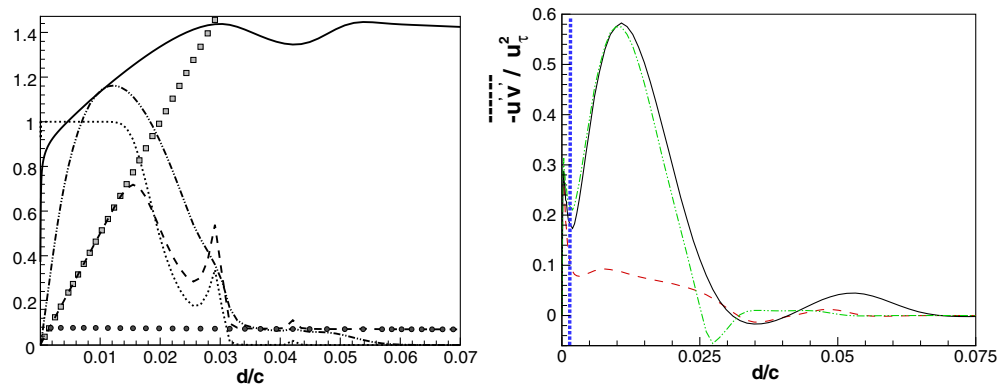

Fig. 11 DDES behavior in the main element boundary layer at $x/c = 0.95$. *Left* —, U/U_∞; – – –, $50\tilde{d}/c$; $\square$, $50d/c$; . . ., $1 - f_d$; — – –, $0.005\mu_t/\mu$; •, $50C_{\text{DES}}\Delta/c$. *Right* modeled Reynolds shear stress; —, RANS; – – –, DES97; — – –, DDES; . . ., interface

notice that the modified length scale $\tilde{d}$ follows the RANS branch farther away from the wall than it would in DES97, being equal to the wall distance d up to $d/c \approx 0.015$, which is more than half of the boundary layer. At its peak, it exceeds $C_{\text{DES}}\Delta$ by an order of magnitude. A second peak at $d/c \approx 0.03$ is due to the shear rate crossing zero and entering r_d in (2.1), but is not noticeably disturbing the eddy viscosity. Figure 11b uses the Reynolds shear stress, as alternative to the eddy viscosity, to reveal the deep differences between DES97 and DDES.

In summary, the cases presented here suggest that the DDES concept is viable, and that the f_d function chosen gives a good enough compromise. Tests conducted on a prolate spheroid are not presented, because present grids are far from fine enough to resolve eddies in the shear layers, so that the switch to LES could not be demonstrated; in addition the grid-induced MSD, which is undesirable, overlaps with the weakening of turbulence by rotation, which is physical and provided by the better RANS models.

4 Some other issues in turbulence simulations

4.1 Wall-modeled LES

The basic DES position [1] was that all turbulent-boundary-layer physics are treated by RANS, so that the accuracy cannot surpass that of the RANS model, including for the prediction of separation which is so crucial. RANS models *will* improve, but the recent pace has been very slow. However, LES offers the possibility of breaking through this "accuracy barrier" of RANS, with fine enough grid and time step, and WMLES offers the possibility of doing so at practical Reynolds numbers. This long-term goal supplied the motivation for the application of the raw DES equations to turbulent channel flow by Nikitin et al. [11]. The backward-facing step

simulations presented above are an example of a DES evolving spontaneously from a RANS into the LES of an attached boundary layer in the downstream region. As outlined in that work [11], the DES equations, with LES grids in the boundary layer (Type III in Fig. 1), provide a wall model for LES and enable LES predictions at unlimited values for the wall-parallel grid spacing in wall units, $\Delta_\parallel^+$. The model is very simple, is robust, and needs no averaging to remain stable, in contrast to some elaborate SGS models. The cost advantage of WMLES over wall-resolved LES, also called Quasi-DNS (in which limits of the order of $\Delta_z^+ \leq 20$ apply [1]) is major at application Reynolds numbers, and WMLES far better meets the spirit of LES [4].

Nikitin et al's [11] exercise showed that WMLES is possible with the DES equations, in the sense that LES content is sustained in the center of the channel, and that wall modeling is achieved, since values of $\Delta_\parallel^+$ such as 8,000 are used with results as accurate as they are at lower Reynolds numbers. At high enough Reynolds number, the mean velocity profiles have a "modeled log layer" near the wall and a "resolved log layer" near the channel center. These layers have about the same Kármán constant κ, for different reasons. The modeled layer returns the Kármán constant contained in the RANS model; the resolved layer returns an accurate value once the grid is fine enough, because LES is performing. The issue is that their intercepts C (in $U^+ = \log(y^+)/\kappa + C$) do not quite match; the layers are not lined up [11]. This issue is referred to as "log-layer mismatch." The presence of this "super-buffer layer" between the RANS and LES regions was expected, and only good fortune could have made the two layers line up perfectly. Recall that no adjustments of any kind were made to the DES formulas, and that the wall-parallel grid spacings Δx and Δz were identical (in other words, knowledge of the skin-friction direction was not used, the way it has been in essentially all previous LES studies). This study was intentionally constrained. The consequence of log-layer mismatch is an under-estimation of the skin-friction coefficient by about 15%, which is not acceptable. This trend may be detected for $x/H \geq 15$ in Fig. 7, confirming that log-layer mismatch is insensitive to the DDES modification. In fact, this mismatch was not a target of the present work; once $f_d = 1$, DDES and DES97 behave the same.

Subsequent studies revealed that straightforward WMLES by the DES model makes the near-wall fluctuations too weak and elongated [10]. A tentative solution is to stimulate this region artificially [24]. This can eliminate the mismatch, at the cost of new adjustable parameters and, more importantly, some coding complexity and some real difficulties controlling this intervention in practical applications. However, recent work has reduced these concerns thanks to a new control strategy [25]. Other solutions are being studied, including non-isotropic eddy viscosities and strong local adjustments of the length scale $\tilde{d}$, but are not sufficiently evolved to be discussed here.

The study of Nikitin et al. [11] appears to have triggered an unfortunate amalgam between DES and WMLES. As an example, Caruelle and Ducros [26] make the nature of their WMLES exercise clear in their text, but not in their title and abstract where only DES is mentioned, so that following contributors may not grasp the essentials of DES. Many WMLES methods use wall models derived from RANS models, which is legitimate. However, the complete method often does not have the ability to treat an entire boundary layer in RANS mode, an ability which is essential to DES. The same distinction exists between the mixing-length model, which extends only into the log layer, and the Baldwin–Lomax model, which extends to the boundary-layer edge and beyond. Methods which use RANS technology only for the purpose of wall modeling in LES have their place, but they are limited, and should not be called "DES."

As far as application of DDES to WMLES is concerned, it has peculiarities. First, the new inter-dependence between the length scale and eddy viscosity field discussed in Sect. 2.2 raises the possibility of multiple solutions in grids suited to WMLES (Type III). This was seen for the two sides of the BFS case and is straightforward to exhibit in a temporal channel flow; even with a grid capable of WMLES, if the initial condition is in the vicinity of a RANS velocity and turbulence field, the solution will continue in RANS mode, i.e., without three-dimensionality or turbulent fluctuations. However, a WMLES can also be obtained, by providing an appropriate initial condition with LES content and low enough eddy viscosity. Multiple solutions are usually not an attractive feature in any method, but here for a mature solution the switch is between two radically different modes, which are obvious in any flow visualization. No LES or DES should be conducted without detailed visualization, a fact which curiously is lost on some users. In tests performed to date, there is no example of a flow alternating between the two modes, or finding an intermediate state at maturity; however, the experience base is still narrow. A DES97 of the channel on a grid of Type II or III with no initial LES content at all would find a pathological state with zero resolved stresses, and weak modeled stresses, which could be very inaccurate and grid-dependent. DDES avoids this pitfall.

Until now, the use of DES as a wall model has taken place only in a channel, removed from natural DES. A long-term goal is to combine the two in the same simulation, such as a flow with both extensive thin boundary layers and a region of thick boundary layer, for instance with incipient separation or recovering after

reattachment. The BFS case is an example. The key to DES preserving a cost advantage over full-domain LES [1] will be to activate WMLES only in turbulent–boundary-layer regions that satisfy two conditions. First, they are challenging due to pressure gradients, active flow control, or other influences, so that the effort is justified. Another motivation exists when a particular region is of special interest for its unsteadiness, causing vibrations or noise. Second, these regions are thick enough compared with their extent that the cost of LES is bearable. The cost predictor used in [1] called N_{cubes}, the number of cubes of size δ needed to fill the turbulent boundary layer, remains valid; formally, N_{cubes} is the integral over the body surface of $1/\delta^2$. The entire boundary layer on a wing may have N_{cubes} of the order of 10^7, because of the thin boundary layer near the leading edge. In contrast, the thick region approaching separation, if its thickness is made to start at 1% of chord, leads to N_{cubes} somewhat over 10^4, under similar assumptions. This is vastly more favorable.

This practice raises a new difficulty, which is not addressed in this paper either. It is the generation of LES content in a boundary layer, with a tolerable recovery region until healthy boundary-layer turbulence is established. The name given by Batten et al. [27] will be used: "Large-Eddy Stimulation (LEST)". The need is not specific to DES, or even to LES; it exists in spatial DNS of a boundary layer, unless transition takes place within the domain. It has long been known that simple random numbers fail to yield a rapid recovery as measured, for instance, by the skin friction. Solutions that construct "turbulence" with combinations of many Fourier modes in time and in the spanwise direction do work better. A successful approach is the rescaling and recycling of unsteady data from a plane somewhat downstream of the inflow plane, proposed by Lund et al. [28]. Simpler versions of this approach also work well [29].

Large-eddy stimulation can take two forms. In most studies, it has been performed at an inflow boundary; the entire domain is in LES mode. However, the capability of generating such eddies *inside* an LES or DES field will be very valuable, as recognized by Batten et al.[27] for LNS . The simulation of a single boundary layer will be in RANS mode up to some line, selected by the user within the attached region, and in LES mode beyond that line. Their position is that the best method will seamlessly stimulate the LES content needed, as the modeled Reynolds stress is vanishing. It is recognized that this will benefit from a sudden grid refinement from Type I to Type III, and will require extra empirical terms in a band of the boundary layer (in contrast with the spontaneous switch at the BFS). However, these terms will be active only over a small volume, in a region that is unchallenging in terms of boundary-layer behavior, and the turbulent boundary layer will lose memory of the details before entering the challenging region, such as an adverse pressure gradient, a step, or a turbulence-control device.

4.2 Low-Reynolds number correction

The low-Reynolds number terms in the S-A RANS model were designed to account for wall proximity, "measured" by the ratio of the eddy and molecular viscosities v_t/v (an expedient to avoid using the friction velocity). Most RANS models have similar terms, also based on various turbulent Reynolds numbers. However, in the LES mode of DES, the subgrid eddy viscosity (normalized by the molecular viscosity) decreases with grid refinement and decrease of the flow Reynolds number. At some point, standard DES will mis-interpret the situation as "wall proximity" and lower the eddy viscosity excessively, relative to the ambient velocity and length scales, through the f_v and f_t functions of the S-A model. Although this deficiency shows up only at relatively low Reynolds numbers and/or with very fine grids, it is still desirable to eliminate it, and to do so without zonal instructions from the user. A correction has been developed for DES97 and tested on a few generic cases, and is given first. DDES is then considered.

The correction to the DES97 formulation reads:

$$l_{\text{DES}} = \min(l_{RANS}, \Psi C_{\text{DES}}\Delta). \qquad (4.3.1)$$

For the S-A model, $l_{\text{DES}} \equiv \tilde{d}$ and $l_{\text{RANS}} \equiv d$. This differs from the original DES97 formulation by the introduction of the factor $\Psi \geq 1$ (without the correction, Ψ would equal 1), which can be interpreted as an increased effective value for C_{DES}. It is a function of v_t/v, or equivalently of the parameter $\chi \equiv \tilde{v}/v$ of the S-A model.

The derivation of the expression for $\Psi(v_t/v)$ is based on the assumption that at "equilibrium" (i.e., when convection and diffusion in the turbulence-transport equations of a RANS model are negligible) the modified subgrid model driven by $l_{\text{DES}} = \Psi C_{\text{DES}}\Delta$ should reduce to a Smagorinski-like model, i.e., $v_t = (C\Delta)^2 S$ where C is constant.
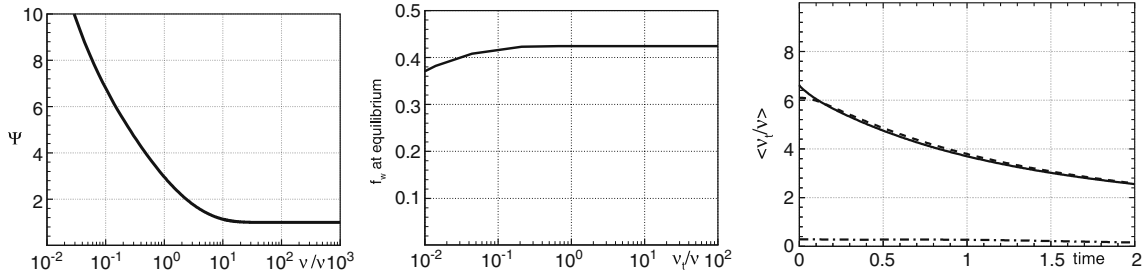
Fig. 12 Low-Reynolds number correction. **a** Ψ function. **b** Equilibrium f_w function. **c** Volume-averaged eddy viscosity in homogeneous turbulence: —, Smagorinski model, - — - DES without correction, - - - DES with correction

Based on this, the following relation for $\Psi(\nu_t/\nu)$ in the S-A based DES97 can be derived:

$$\Psi^2 = \frac{\frac{f_w}{f_w^*} - \frac{c_{b1}}{c_{w1}\kappa^2 f_w^*}[f_{t2} + (1 - f_{t2})f_{v2}]}{f_{v1}(1 - f_{t2})}. \tag{4.3.2}$$

This function is shown in Fig. 12a. All the notations in the right-hand side of (4.3.2), except for the quantity f_w^*, are the same as in the S-A model [8]. Note that the "equilibrium" function f_w in (4.3.2) can be shown to satisfy the following nonlinear algebraic equation:

$$f_w = \phi\left(g[r(f_w, \chi)]\right), \qquad r(f_w, \chi) = \frac{c_{b1}(1 - f_{t2})}{\kappa^2 c_{w1} f_w - c_{b1} f_{t2}}, \qquad \phi(g) \equiv g\left(\frac{1 + c_{w3}^6}{g^6 + c_{w3}^6}\right)^{1/6} \tag{4.3.3}$$

and therefore is a function of χ (or ν_t/ν) only. The quantity f_w^* in (4.3.2) is the limit value of the function f_w defined by (4.3.3) at high subgrid viscosity, $\nu_t \gg \nu$, i.e., at high cell Reynolds number. Its value is $f_w^* = 0.424$.

The solution of (4.3.3), shown in Fig. 12b, shows that the ratio f_w/f_w^* is a weak function of ν_t/ν; for the meaningful range of eddy viscosity, $\nu_t > \nu/10$, it is equal to 1 within 2%. This allows the replacement of expression (4.3.2) for Ψ by:

$$\Psi^2 = \min\left[10^2, \frac{1 - \frac{c_{b1}}{c_{w1}\kappa^2 f_w^*}[f_{t2} + (1 - f_{t2})f_{v2}]}{f_{v1}\max(10^{-10}, 1 - f_{t2})}\right]. \tag{4.3.4}$$

in which Ψ and $1 - f_{t2}$ are now limited from above and below to ensure reasonable behavior of Ψ in the "DNS limit" $\nu_t < \nu/100$. The correction is inactive ($\Psi = 1$) for a subgrid eddy viscosity higher than about 10ν, and becomes quite strong for lower values. This modification of S-A DES97 has been successfully applied to the homogeous-turbulence problem, to the cylinder flow, and to the NACA 0012 airfoil at 60° angle of attack [30]. The eddy viscosity in a 64^3-grid LES of homogeneous isotropic turbulence is shown in Fig. 12c, and the effect of Ψ is large; note that the eddy viscosity is a few times the molecular viscosity.

The same methodology may be applied for designing corrections to any other DES versions based on RANS models that include low-Reynolds number terms. For instance, for the Wilcox k-ω model [31][1], it results in the following expression for Ψ:

$$\Psi = \Psi(Re_t) = \frac{\beta^*}{C_\mu}\left(\frac{2\alpha}{\alpha^*}\right)^{3/4},$$

where $Re_t \equiv k/(\omega\nu)$ is the turbulent Reynolds number, and C_μ, α, α^* and β^* are the constants and "low-Reynolds-number" functions of the model.

The above approach is of course applicable to DDES as well. However in this case the f_d function is also available to correct at low cell Reynolds numbers. For instance, in the S-A based DDES, the variable χ is replaced with $\max(\chi, 20f_d)$ before entering the functions f_{v1} and f_{t2}.

---

[1] The corresponding subgrid model can be obtained from the RANS model exactly the same way as it was done in [20] for the SST model, i.e., by replacement of l_{RANS} with $\Psi C_{DES}\Delta$ in the dissipation term of the k-transport equation only (the C_{DES} value defined by calibration on the decaying isotropic homogeneous turbulence problem for this model is 0.72).

5 Outlook

The new version of DES proposed here was prompted by independent findings of users, was guided by work of Menter and Kuntz [14] and is supported in this paper by a fair set of tests, in different codes. Although it cannot be that the absolute best formulation was found, the present one for f_d appears simple and permanent enough to be recommended. It also fits the spirit of DES as introduced in 1997; the formulas changed and now involve the solution in the definition of $\tilde{d}$, unlike before, but the intent has not changed. The MSD phenomenon that is suppressed on ambiguous grids is definitely spurious, and loss of LES behavior after massive separation has not been observed. Whereas with DES97, MSD is encountered with grid densities that are practical at least in thick boundary layers, DDES would suffer MSD only in extreme grids. The code modification is not very inconvenient. The increased possibility of multiple solutions is not a major issue, and would be problematic only if DES were used as a "black box."

References

1. Spalart, P.R., Jou, W.-H., Strelets, M., Allmaras, S.R.: Comments on the feas1ibility of LES for wings, and on a hybrid RANS/LES approach. In: Proceedings of first AFOSR international conference on DNS/LES, Ruston, Louisiana. Greyden Press, 4–8 Aug (1997)
2. Shur, M., Spalart, P.R., Strelets, M., Travin, A.: Detached-eddy simulation of an airfoil at high angle of attack. In: proceedings of 4th international symposium on engineering turbulence modelling and measurements, Corsica. Elsevier, 24–26 May (1999)
3. Travin, A., Shur, M., Strelets, M., Spalart, P.: Detached-eddy simulations past a circular cylinder. Flow Turb Comb **63**, 293 (2000)
4. Spalart, P.: Strategies for turbulence modelling and simulations. Int. J. Heat Fluid Flow. **21**, 252 (2000)
5. Spalart, P.R.: Young person's guide to detached-eddy simulation grids. NASA CR-2001-211032
6. Deck, S., Garnier, E.: Detached and large eddy simulation of unsteady side-loads over an axisymmetric afterbody. In: Proceedings of 5th European Symposium on aerothermodynamics for space vehicles. Cologne, Germany, 8–11 November (2004)
7. Mellen, C.P., Frölich, J., Rodi, W.: Lessons from the European LESFOIL project on LES of flow around an airfoil. AIAA J. **41**(4), 573–581 (2003)
8. Spalart, P.R., Allmaras, S.R.: A one-equation turbulence model for aerodynamic flows. La Rech. Aérospatiale **1**, 5–21 (1994)
9. Breuer, M., Jovičić, N., Mazaev, K.: Comparison of DES, RANS and LES for the separated flow around a flat plate at high incidence. Int. J. Num. Meth. Fluids. **41**, 357–388 (2003)
10. Piomelli, U., Balaras, E.: Wall-layer models for large-eddy simulations. Ann. Rev. Fluid Mech. **34**, 349–374 (2002)
11. Nikitin, N.V., Nicoud, F., Wasistho, B., Squires, K.D., Spalart, P.R.: An approach to wall modeling in large-eddy simulations. Phys. Fluids **12**, 7 (2000)
12. Caruelle, B.: Simulations d'écoulements instationnaires turbulents en aérodynamique: application à la prédiction du phénomène de tremblement. PhD. thesis, INPT/CERFACS (2000)
13. Deck, S.: Simulation numérique des charges latérales instationnaires sur des configurations de lanceur. PhD thesis, U. Orléans (2002)
14. Menter, F.R., Kuntz, M.: Adaptation of eddy-viscosity turbulence models to unsteady separated flow behind vehicles. In: McCallen, R., Browand, F., Ross, J. (eds.) Symposium on "the aerodynamics of heavy vehicles: trucks, buses and trains." Monterey, USA, 2–6 Dec 2002, Springer, Berlin Heidelberg New York (2004)
15. Batten, P., Goldberg, U., Chakravarthy, S.: LNS – an approach towards embedded LES. AIAA-2002-0427
16. Menter, F.R., Kuntz, M., Bender, R.: A scale-adaptive simulation model for turbulent flow predictions. AIAA 2003-0767
17. Travin, A., Shur, M., Spalart, P., Strelets, M.: On URANS solutions with LES-like behaviour. In: Proceedings of ECCOMAS congress on Computational Methods in Applied Science and Engineering, Jyväskylä, Finland, 24–28 July (2004)
18. Deck, S., Garnier, E., Guillen, P.: Turbulence modelling applied to space launcher configurations. J. Turbulence **3** (2002)
19. Forsythe, J.R., Fremaux, C.M., Hall, R.M.: Calculation of static and dynamic stability derivatives of the F/A-18E in abrupt wing stall using RANS and DES. In: Proceedings of 3rd International Conference on CFD, Toronto, July (2004)
20. Travin, A., Shur, M., Strelets, M., Spalart, P.R.: Physical and numerical upgrades in the detached-eddy simulation of complex turbulent flows. In: Friedrich, R., Rodi, W. (eds.), Proceedings of Euromech Coll. 412 "LES of complex transitional and turbulent flows," Munich, Germany, 5–6 October 2000. Kluwer, Dordrecht (2002)
21. Cantwell, B., Coles, D.: An experimental study of entrainment and transport in the turbulent near wake of a circular cylinder. J. Fluid Mech. **136**, 321–374 (1983)
22. Gleyzes, C., Capbern, P.: Experimental study of two AIRBUS/ONERA airfoils in near stall conditions. Aerosp. Sci. Technol. **7**, 439–449 (2003)
23. Vogel, J.C., Eaton, J.K.: Combined heat transfer and fluid dynamic measurements downstream of a backward-facing step. J. Heat Mass Transfer. (Trans. ASME) **107**, 922–929 (1985)
24. Piomelli, U., Balaras, E., Pasinato, H., Squires, K.D., Spalart, P.R.: The inner-outer layer interface in large-eddy simulations with wall-layer models. Int. J. Heat Fluid Flow **24**, 538–550 (2003)

25. Keating, A., Piomelli, U.: A dynamic stochastic forcing method as a wall-layer model for large-eddy simulations. To appear, J. Turb. (2006) (in press)
26. Caruelle, B., Ducros, F.: Detached-eddy simulations of attached and detached boundary layers. Int. J. Comp. Fluid Dyn. **17**(6), 433–451 (2003)
27. Batten, P., Goldberg, U., Chakravarthy, S.: Interfacing statistical turbulent closures with large-eddy simulation. AIAA J. **42**(3), 485–492 (2004)
28. Lund, T.S., Wu, X., Squires, K.D.: Generation of turbulent inflow data for spatially-developing boundary layer simulations. J. Comp. Phys. **140**, 233–258 (1998)
29. Spalart, P.R., Strelets, M., Travin, A.: Direct numerical simulation of large-eddy-break-up devices in a boundary layer. In: Rodi, W. (ed.) Proceedings of 6th international symposium on engineering turbulance modelling and measurements. 4 May 2005, Sardinia. Int. J. Heat Fluid Flow (2006) (in press)
30. Shur, M.L., Spalart, P.R., Strelets, M., Travin, A.: Modification of S-A subgrid model in DES aimed to prevent activation of the low-Re terms in LES mode. In: Proceedings of workshop on DES, St.-Petersburg, http://cfd.me.umist.ac.uk/flomania, 2–3 July (2003)
31. Wilcox, D.C.: Turbulence modeling for CFD. 2nd edn. DCW Indus., La Cañada, CA (1998)